Global-local ansatz and dynamical coherent potential approximation study of off-diagonal exciton-phonon coupling

Liu, Qingmei; Zhao, Yang; Wang, Weihua; Kato, Tsuyoshi

2009

Liu, Q., Zhao, Y., Wang, W., & Kato, T. (2009). Global-local ansatz and dynamical coherent potential approximation study of off-diagonal exciton-phonon coupling. Physical review B, (79), 1-14.

https://hdl.handle.net/10356/99800

https://doi.org/10.1103/PhysRevB.79.165105

Global-local ansatz and dynamical coherent potential approximation study of off-diagonal exciton-phonon coupling

Qingmei Liu,[1] Yang Zhao,[1,*] Weihua Wang,[1,2] and Tsuyoshi Kato[3]
[1]*School of Materials Science and Engineering, Nanyang Technological University, Singapore 639798, Singapore*
[2]*Department of Electronics, College of Information Technical Science, Nankai University, Tianjin 300071, China*
[3]*Department of Chemistry, School of Science, University of Tokyo, Hongo Bunkyo-ku, Tokyo 113-0033, Japan*
(Received 14 December 2008; published 10 April 2009)

We study the generalized Holstein Hamiltonian in the simultaneous presence of diagonal and off-diagonal exciton-phonon couplings using the global-local Ansatz and the dynamical coherent potential approximation (under the Hartree approximation). The former yields detailed exciton-phonon correlations for polaron states in the lowest polaron energy band in addition to the state-of-the-art ground-state wave functions, while the latter reveals polaron dynamic information in the form of extended energy spectra and spectral density functions. Lowest polaron energy bands generated by the two methods are compared.

DOI: 10.1103/PhysRevB.79.165105 PACS number(s): 71.35.Aa, 72.10.Di

I. INTRODUCTION

We revisit a classic problem of polaron theory in one dimension incorporating diagonal and off-diagonal exciton-phonon couplings. The ground-state and dynamic properties of a Holstein polaron depend on resonance transfer integrals among exciton states, characteristics of the phonon bath, and in particular, mechanisms and strengths of exciton-phonon coupling. Diagonal exciton-phonon coupling is defined as a nontrivial dependence of the exciton site energies on the lattice coordinates, and off-diagonal coupling is defined as a nontrivial dependence of the exciton transfer integral on the lattice coordinates.[1–3] Off-diagonal coupling is expected to play an important role in organic molecular crystals of polyacenes (such as naphthalene, anthracene, and tetracene), for which the electronic transfer integral depends strongly on optical phonons (especial those of rotational provenance[4]). Simultaneous diagonal and off-diagonal couplings can also be important in the characterization of solid-state excimers, where a variety of experimental and theoretical considerations suggests that a strong dependence of electronic tunneling upon certain coordinated distortions of neighboring molecules (or off-diagonal exciton-phonon coupling) is crucial to the formation of the excited bounded states.[5,6]

Much attention has been devoted to the Holstein molecular crystal model using various theoretical methods such as density-matrix renormalization group (DMRG),[7] variational approaches,[8,9] cluster diagonalization,[10] dynamical mean-field theory (DMFT),[11] and quantum Monte Carlo (QMC).[12] The DMRG method is generally regarded as a benchmark for calculating the ground-state energy, although it fails to yield a trial wave function at the end of the computation due to a constantly changing basis set in iteration. A comprehensive comparison of various methodologies for the ground-state energy and the effective polaron mass shows that the global-local (GL) Ansatz[8] is the state-of-the-art polaron wave function with precision matching that of the computationally much more expensive DMRG method. A few dynamical approaches,[13–16] such as momentum average (MA) and QMC, have been applied to study spectral properties of the Holstein Hamiltonian. In Ref. 13, for example, the diagrammatic QMC approach is based on the Feynman expansion of the Matsubara Green's function in imaginary time in the interaction representation, followed by an analytic continuation to real frequencies. Additionally, the MA method[14,16] is an analytical method to simplify the momentum-dependent self-energy. However, most of the existing work is concerned solely with diagonal exciton-phonon coupling. Little attention has been paid to the off-diagonal coupling. Therefore, it is necessary to develop numerical methods to study a generalized Holstein molecular crystal model with simultaneous diagonal and off-diagonal exciton-phonon couplings.

The one-dimensional (1D) generalized Holstein Hamiltonian with simultaneous diagonal and off-diagonal couplings to Einstein phonons has been previously modeled by the Munn-Silbey approach[1,3] and by a variational wave function pioneered by Toyozawa.[2,17] Since the Munn-Silbey method is based on a perturbative assumption with the coefficients of a canonical transformation being so determined as to limit the secular growth with the temperature of the perturbation remaining after transformation, it cannot adequately describe the polaron states at low temperatures. Furthermore, the self-consistency equations in the Munn-Silbey method do not include the exciton transfer integral; therefore, it is limited to the narrow-band regime. Subsequently, the Toyozawa Ansatz was used to overcome aforementioned limitations of the Munn-Silbey method. The Toyozawa Ansatz was later made more accurate by the GL Ansatz, which takes into account both phonon displacements independent of the exciton location and those dependent on the distance between the exciton and the phonons. Our previous work on cases with only diagonal exciton-phonon coupling shows that the GL Ansatz is comparable in ground-state energy accuracy with the DMRG method.[8] Therefore, it is desirable to extend the GL Ansatz to include off-diagonal coupling and compare results with various other methods.

The generalized Holstein Hamiltonian can also be tackled by the dynamical coherent potential approximation in combination with the Hartree approximation (HA-DCPA),[18] an extension of the original dynamical coherent potential approximation (DCPA) pioneered by Sumi.[19] Though the DCPA approach can systematically treat the multiple inelas-

tic scattering of an exciton by phonons, it is limited to the case of diagonal coupling due to a single-site approximation. Kato *et al.*[18,20] extended Sumi's DCPA to treat more general exciton-phonon systems with dispersive phonons, off-diagonal coupling, and multiexcitons. The basic idea of HA-DCPA is to assume a momentum-dependent coherent potential for exciton-phonon scattering and a perturbative scattering matrix that vanishes under thermal averages, and consequently a self-consistency equation on the one-exciton Green's function can be formulated.

In this paper, we study a generalized molecular crystal model in one dimension with simultaneous diagonal and off-diagonal exciton-phonon couplings using both the HA-DCPA method and the GL Ansatz. In Sec. II, the generalized Holstein Hamiltonian is introduced. In Sec. III, a detailed description of the HA-DCPA method is given, and the GL Ansatz is formulated for the simultaneous presence of diagonal and off-diagonal couplings. In Sec. IV, calculation results from the two approaches are presented and compared. Conclusions are drawn in Sec. V.

II. MODEL HAMILTONIAN

The traditional molecular crystal model of Holstein describes a lattice of two energy-level molecules interacting with a bath in one-dimensional space,[21,22]

$$\hat{H} = \hat{H}^{\text{ex}} + \hat{H}^{\text{ph}} + \hat{H}^{\text{ex-ph}}, \tag{1}$$

$$\hat{H}^{\text{ex}} = -J\sum_n a_n^\dagger (a_{n+1} + a_{n-1}), \tag{2}$$

$$\hat{H}^{\text{ph}} = \hbar\omega \sum_n b_n^\dagger b_n, \tag{3}$$

$$\begin{aligned}\hat{H}^{\text{ex-ph}} &= g\hbar\omega\sum_n a_n^\dagger a_n (b_n^\dagger + b_n) \\ &+ \frac{\phi}{2}\hbar\omega\sum_n (a_n^\dagger a_{n-1} + a_{n-1}^\dagger a_n - a_{n+1}^\dagger a_n - a_n^\dagger a_{n+1}) \\ &\times (b_n^\dagger + b_n),\end{aligned} \tag{4}$$

in which $a_n^\dagger$ creates an exciton in the rigid-lattice Wannier state at site n and $b_n^\dagger$ creates a quantum of vibrational energy in the Einstein oscillator at site n. Both the excitons and phonons are treated as bosons. The Einstein frequency is given by ω, J is the exciton transfer integral between nearest-neighbor sites, g is the diagonal-coupling strength, and ϕ is the off-diagonal coupling strength characterizing phonon-assisted transfers between nearest-neighbor sites. Throughout this paper, we use the optical phonon frequency as the energy unit so that all energies are dimensionless. In the adiabatic regime, it is convenient to select the exciton half-bandwidth zJ as the unit of energy, where z is the site coordination number (for example, $z=2$ in 1D). Then the remaining dimensionless control parameters are the phonon energy $\gamma = \hbar\omega/2J$ and the exciton-phonon interaction energy $\sqrt{\gamma/\lambda}$, where $\lambda = g^2\hbar\omega/2J$.

Also throughout this paper, we use the Fourier transformations for ladder operators $c^\dagger = a^\dagger$, $b^\dagger$, etc., and scalars $\gamma = \alpha$, β, etc.,

$$c_n^\dagger = N^{1/2}\sum_p e^{-ipn} c_p^\dagger, \quad c_p^\dagger = N^{1/2}\sum_n e^{ipn} c_n^\dagger, \tag{5}$$

$$\gamma_n = N^{-1}\sum_p e^{ipn}\gamma_p, \quad \gamma_p = \sum_n e^{-ipn}\gamma_n. \tag{6}$$

We indicate exciton and phonon wave vectors by Latin indices and reserve the Greek κ for the joint crystal momentum; however, to simplify presentation we suppress the explicit κ label on many quantities since the relevant value is generally clear from context.

After adopting those Fourier transformations of exciton or phonon operators, the generalized Holstein Hamiltonian in the momentum space can be written as follows:

$$\hat{H}^{\text{ex}} = \sum_k \epsilon_k a_k^\dagger a_k = -2J\sum_k \cos(k) a_k^\dagger a_k, \tag{7}$$

$$\hat{H}^{\text{ph}} = \sum_q b_q^\dagger b_q, \tag{8}$$

$$\hat{H}^{\text{ex-ph}} = \sum_q \hat{H}'_q, \tag{9}$$

$$\hat{H}'_q = \sum_{k,k'} (f_{k,k'}^q b_q^+ + \tilde{f}_{k,k'}^q b_q) a_k^\dagger a_{k'}, \tag{10}$$

$$f_{k,k'}^q = \frac{1}{\sqrt{N}}\{g\,\delta_{k,k'} + i\phi[\sin(k) - \sin(k')]\}, \tag{11}$$

where the index q represents phonon modes, and k and k' are discrete indices in the momentum space.

III. METHODOLOGY

In this section we give a detailed description of the two approaches to treat the Holstein model with simultaneous diagonal and nondiagonal couplings, namely, the HA-DCPA method[18] and the GL Ansatz.[8]

A. HA-DCPA method

The coherent potential approximation (CPA) was originally put forward by Soven[23] and Taylor[24] to study elastic impurity scattering of disordered alloys. In this approach, the propagation of an electron in a disordered alloy is regarded as a succession of elementary scatterings off random atomic scatters, which are then averaged over all atomic configurations. A given electron is viewed to be embedded in an effective medium, which can be self-consistently determined. The basic assumption is that a single scatterer embedded in this effective medium should produce no further scattering on the average.[25] Sumi later extended this approach to study exciton-phonon systems by taking inelastic scatterings into account under a single-site approximation.

Our main objective is to calculate the one-exciton Green's function by introducing an energy-dependent, translationally invariant, and nonlocal coherent potential $V_{k,k'}$ to describe dynamical exciton-phonon correlations.[26] The original Hamiltonian is divided into two parts, the effective Hamiltonian $\hat{H}_{\text{eff}}$ and the perturbation term $\hat{H}_{\text{pert}}$,

$$\hat{H} = \hat{H}_{\text{eff}} + \hat{H}_{\text{pert}}, \tag{12}$$

$$\hat{H}_{\text{eff}} = \sum_{k,k'} (\epsilon_k \delta_{k,k'} + V_{k,k'}) a_k^\dagger a_{k'} + \hat{H}_{\text{ph}}, \tag{13}$$

$$\hat{H}_{\text{pert}} = \hat{H}^{\text{ex-ph}} - \sum_{k,k'} V_{k,k'} a_k^\dagger a_{k'} \tag{14}$$

$$\equiv \sum_q \hat{U}^q, \tag{15}$$

where the effective Hamiltonian $\hat{H}_{\text{eff}}$ includes the zeroth-order exciton and phonon Hamiltonians, and the perturbation $\hat{H}_{\text{pert}}$ is written as a sum of auxiliary operators $\hat{U}^q$ over momentum q,

$$\hat{U}^q = \hat{H}'_q - \sum_{k,k'} V^q_{k,k'} a_k^\dagger a_{k'}. \tag{16}$$

Here the total coherent potential $V_{k,k'}$ is assumed to be written as a summation of contributions from individual phonon modes,[25]

$$V_{k,k'} = \sum_q V^q_{k,k'}. \tag{17}$$

The partial coherent potential $V^q_{k,k'}$ from the qth phonon mode will be determined by a set of self-consistency equations. CPA is an effective method to calculate polaron self-energy functions by taking into account multiphonon scattering nonperturbatively, and our task here is to self-consistently determine the effective medium corresponding to $\hat{H}_{\text{eff}}$. $\hat{T}$-matrix operators are used to describe scattering of the excitons in the effective field $\hat{H}_{\text{eff}}$ by the perturbation $\hat{H}_{\text{pert}}$. Similar to the conventional CPA or DCPA, the coherent potential $V_{k,k'}$ is chosen such that, with $\hat{H}_{\text{eff}}$ as the unperturbed Hamiltonian and $\hat{H}_{\text{pert}}$ as the perturbation, the thermally averaged $\hat{T}$ matrix vanishes (details of the T matrix will be given shortly afterwards).

Let us first define the thermally averaged retarded one-exciton Green's function

$$iG_{k,k'}(t) = \theta(t)\langle \exp(i\hat{H}t) a_k \exp(-i\hat{H}t) a_{k'}^+ \rangle, \tag{18}$$

where $\theta(t)$ is the unit step function and $\langle\ \rangle$ denotes the canonical average over the phonon population at temperature $1/\beta$. The Fourier transformation of the Green's function has the form

$$G_{k,k'}(\omega) = \int_{-\infty}^{\infty} dt \exp(i\omega t) G_{k,k'}(t), \tag{19}$$

with imaginary part of ω as positive infinitesimal.

According to the aforementioned decomposition of the Hamiltonian, we can write a Dyson equation in terms of the retarded one-exciton Green's function,

$$G_{\text{eff}}(z) = \frac{1}{z - \epsilon_k - V(z)}, \tag{20}$$

$$G_o = G_{\text{eff}} + G_{\text{eff}} \langle T \rangle G_{\text{eff}}, \tag{21}$$

where the complex energy z is composed of the exciton energy E and the exciton damping constant $\eta > 0$ such that $z = E + i\eta$, and the $V(z)$ matrix stands for the coherent potential $V_{k,k'}$. G_o is the Green's function associated with the original Hamiltonian $\hat{H}$, and G_{eff} corresponds to the effective Hamiltonian $\hat{H}_{\text{eff}}$. The $\hat{T}$-matrix operator is used to describe the scattering of the excitons in the effective field $\hat{H}_{\text{eff}}$ by the perturbation $\hat{H}_{\text{pert}}$. Self-consistency is achieved with $G_o = G_{\text{eff}}$ if $\langle \hat{T} \rangle = 0$. In general, however, it is difficult to make the $\hat{T}$ matrix vanish entirely. Only under certain conditions, such as using the single-site approximation or adopting a cluster generalization of DCPA,[27] one can solve the self-consistency equation for the single-particle Green's function.

We first decompose the $\hat{T}$ matrix as follows:

$$\hat{T} = \sum_q \hat{t}^q + \sum_q \sum_{q' \neq q} \hat{t}^q G_{\text{eff}} \hat{t}^{q'} \tag{22}$$

$$+ \sum_q \sum_{q' \neq q} \sum_{q'' \neq q' \neq q} \hat{t}^q G_{\text{eff}} \hat{t}^{q'} G_{\text{eff}} \hat{t}^{q''} + \cdots, \tag{23}$$

where $\hat{t}^q$ denotes the partial scattering matrix with the unperturbed Hamiltonian $\hat{H}_{\text{eff}}$ and a perturbation $\hat{U}^q$,

$$\hat{t}^q = \hat{U}^q + \hat{U}^q G_{\text{eff}} \hat{U}^q + \hat{U}^q G_{\text{eff}} \hat{U}^q G_{\text{eff}} \hat{U}^q + \cdots. \tag{24}$$

We neglect phonon mode correlations using the Hartree approximation, e.g.,

$$\langle \hat{t}^q G_{\text{eff}} \hat{t}^{q'} \rangle = \langle \hat{t}^q \rangle G_{\text{eff}} \langle \hat{t}^{q'} \rangle \quad (q' \neq q). \tag{25}$$

It follows that the self-consistency condition $\langle \hat{T} \rangle = 0$ is simplified to $\langle \hat{t}^q \rangle = 0$, i.e., each partial scattering matrix $\hat{t}^q$ vanishes under thermal averages. This approximation is analogous to the decoupling scheme used in the single-site DCPA,

$$\langle \hat{t}_i G_{\text{eff}} \hat{t}_j \rangle = \langle \hat{t}_i \rangle G_{\text{eff}} \langle \hat{t}_j \rangle \quad (i \neq j), \tag{26}$$

where i and j are site indices and $\hat{t}_i$ denotes single-site $\hat{T}$ matrix relative to the effective Hamiltonian. Any spatial correlations beyond the single-site multiple scattering described by $\hat{T}$ matrix are neglected in this approximation.[28] At zero temperature, $\langle \hat{t}^q \rangle$ has to vanish after averaging in the phonon vacuum.

The condition that every $\hat{t}^q$ matrix vanishes under thermal averages, or that the multiple scattering from each phonon

mode described by $\hat{U}^q$ vanishes on the average, allows V^q to be determined. Thus it is sufficient to investigate a Hamiltonian $\hat{H}^q$, for which only exciton-phonon scattering from one specified phonon mode q is considered with the rest of the phonon modes q' $(q' \neq q)$, providing an effective mean field of $V-V^q$,

$$\hat{H}^q = \hat{h}^{(q)}(z) + \hat{H}'_q, \tag{27}$$

$$\hat{h}^{(q)}(z) = \hat{H}_{\text{eff}} - \sum_{k,k'} [V^q(z)_{k,k'}] a_k^\dagger a_{k'}, \tag{28}$$

where $\hat{H}'_q$ is given by Eq. (10). According to the decomposition of $\hat{H}^q$, an operator identity holds[29]

$$\frac{1}{z-\hat{H}^q} = \frac{1}{z-\hat{h}^{(q)}} + \frac{1}{z-\hat{h}^{(q)}} \hat{H}'_q \frac{1}{z-\hat{H}^q}. \tag{29}$$

Making use of $\hat{h}^{(q)}(z)$, we can define $g_0^q(z)$ as the effective free propagator in an effective mean field $V-V^q$ and $g^{(q)}(z)$ as the thermal average of the Green's function associated with the Hamiltonian $\hat{H}^q$. That is, once all exciton-phonon scattering contributions from phonon modes q' $(q' \neq q)$ are summed, one obtains the free propagator $g_0^q(z)$; if the remaining contribution from the phonon mode q is taken into account, the Dyson equation with respect to $V^q(z)$ will assume the form

$$[g_0^q(z)]^{-1} = [g^{(q)}(z)]^{-1} + V^q(z). \tag{30}$$

The Green's function $g^{(q)}(z)$ can be explicitly written as

$$g^{(q)}(z) = G_{\text{eff}} + G_{\text{eff}} \langle \hat{t}^q \rangle G_{\text{eff}}. \tag{31}$$

Assuming $\langle \hat{t}^q \rangle = 0$, a self-consistency equation then follows

$$g^{(q)} = G_{\text{eff}}. \tag{32}$$

This equation implies that the scattering of an exciton in an effective field $\hat{H}_{\text{eff}}$ associated with the coherent potential V is the same as the scattering of an exciton by phonons in the auxiliary potential $V-V^q$, which is induced by the coupling with all the phonon modes other than the relevant coupling mode q.[18] Both $g^{(q)}(z)$ and G_{eff} may be expressed as a function of V^q, which would be determined self-consistently by a continued-fraction technique as described below.

The perturbative part $\hat{H}'_q$ can be expanded in the phonon-number representation, and a complete basis set of exciton-vacuum p-phonon states $|0,p\rangle$ (Refs. 11 and 30) are inserted into $\hat{H}'_q$,

$$\hat{H}'_q = \sum_{k,k'} \sum_p a_k^\dagger |0,p\rangle\langle 0,p| (f^q_{k,k'} b_q^+ + \tilde{f}^q_{k,k'} b_q) a_{k'}. \tag{33}$$

By substituting $\hat{H}'_q$ into Eq. (29), we obtain a recursive relation for $g_0^q(z)$,

$$g^q(z)_{m,l} = g_0^q(z-m)_{0,m} \delta_{m,l} + \sum_p g_0^q(z-m)_{0,m} X^q_{m,p} g^q(z)_{p,l}, \tag{34}$$

$$X^q_{m,p} = \sqrt{p+1}\, \delta_{m,p+1} F^q + \sqrt{p}\, \delta_{m,p-1} \tilde{F}^q, \tag{35}$$

where F^q and $\tilde{F}^q$ are the matrices denoting $\{f^q_{k,k'}\}$ and $\{\tilde{f}^q_{k,k'}\}$, respectively. Consequently, $g_0^q(z)^{-1}$ is recognized as a tridiagonal matrix due to the recurrence relations of matrix $X_{m,p}$, and the corresponding coherent potential V^q can be written in terms of a continued-fraction expansion as a function of the effective free propagator $g_0^q(z)$,

$$V^q(z) = F^q \frac{1}{[g_{01}^{(q)}]^{-1} - F^q \dfrac{2}{[g_{02}^{(q)}]^{-1} - \cdots}} \tilde{F}^q,$$

where $g_{0i}^{(q)}$ is defined as

$$g_{0i}^{(q)} = g_0^{(q)}(z-i) \quad (i = 1,2,3,\ldots). \tag{36}$$

The coherent potential V and the effective Green's function G_{eff} can thus be solved by an iterative procedure. In the iteration, the coherent potential $V(z)$ at energy z is calculated from those at lower energies $V(z-i)$ $(i=1,2,\ldots)$, and a truncation is necessary to limit the maximum number of phonons participating in the scattering process at $n_{\max}$. The coherent potential at energies outside the chosen window, such as $V(z-n_{\max})$, is assumed to vanish so that at those energies the system behaves as a free exciton sans exciton-phonon coupling. The noninteracting one-exciton Green's function $g_0^{(q)}$ is used initially as a first guess to compute a set of potentials V^q and to update $g_0^{(q)}$. The updated $g_0^{(q)}$ is then fed into the iteration to arrive at the coherent potentials V^q for the next energy point.

Once the coherent potential matrix V is determined, the spectral density function $A(k,E)$ and the polaron energy band $E(k)$ can be evaluated,

$$A(k,E) = -\frac{1}{\pi} \text{Im}[G(k,E)], \tag{37}$$

$$E(k) = \epsilon_k + V(z)_{k,k}. \tag{38}$$

In the numerical implementation, further approximations are made to reduce memory and CPU costs. For example, if K and N denote the number of points the Brillouin zone and in the chosen energy window, respectively, then we need to store $K^2 N n_{\max}$ complex matrix elements for $g_0^{(q)}$ and auxiliary matrices. In the iterative procedure employed to calculate the coherent potentials V^q, adjacent energy points are separated by a spacing of 0.002. In most of our calculations, the number of discrete K points in the first Brillouin zone is taken as 32 for comparison with results from the GL method. We keep the maximum phonon number $n_{\max}$ up to 60 so that errors from the phonon-number truncation are negligible.

B. Variational approach

Generally speaking, variational approaches such as the Merrifield[31] and Toyozawa Ansätze aim to achieve a set of optimized polaron correlations through searching the parameter space. To better describe the principal exciton-phonon correlation channels, the GL Ansatz decomposes the phonon

amplitudes into two parts, and in the site-space representation, the trial state can be written as

$$|\Psi(\kappa)\rangle = N^{-1/2}\sum_n e^{i\kappa n}\sum_{n_1}\psi^{\kappa}_{n_1-n}a^{\dagger}_{n_1} \times\exp\left\{-\sum_{n_2}[(\alpha^{\kappa}_{n_2-n}-\beta^{\kappa}_{n_2-n_1})b^{\dagger}_{n_2}-\text{H.c.}]\right\}|0\rangle, \tag{39}$$

where H.c. is short for Hermitian conjugate, ψ^{κ}_n is the exciton amplitude, and the two-parameter phonon displacement,[3,8,32] $\alpha^{\kappa}_{n_2-n}-\beta^{\kappa}_{n_2-n_1}$, generalizes its one-parameter counterpart in the Toyozawa Ansatz. $\alpha^{\kappa}_{n_2-n}$ represents the part of the phonon displacement independent of the location of the electronic excitation (as in the Toyozawa Ansatz), and $\beta^{\kappa}_{n_2-n_1}$ represents the part that only depends on the relative separation between the phonon and the electronic excitation.

Owing to practical considerations, the form of trial state actually uses the hybrid real-space/reciprocal-space representation[8,32]

$$|\Psi(\kappa)\rangle = N^{-1/2}\sum_{nn_1} e^{i\kappa n}\psi^{\kappa}_{n_1-n}a^{\dagger}_{n_1} \times\exp\left\{-\sum_q[(\alpha^{\kappa}_q e^{-iqn}-\beta^{\kappa}_q e^{-iqn_1})b^{\dagger}_q-\text{H.c.}]\right\}|0\rangle. \tag{40}$$

We note that the GL Ansatz is not normalized,

$$M^{\kappa} = \langle\Psi(\kappa)|\Psi(\kappa)\rangle = \sum_{nm} e^{-i\kappa n}\psi_m\psi^*_{m-n}S^0_{nm}. \tag{41}$$

Next, the expectation values of the three terms in the Holstein Hamiltonian can be evaluated as

$$\langle\Psi(\kappa)|\hat{H}^{\text{ex}}|\Psi(\kappa)\rangle = -J\sum_{nm} e^{-i\kappa n}\psi_m(\psi^*_{m-n+1}S^{+1}_{nm}+\psi^*_{m-n-1}S^{-1}_{nm}), \tag{42}$$

$$\langle\Psi(\kappa)|\hat{H}^{\text{ph}}|\Psi(\kappa)\rangle = N^{-1}\sum_{nmq} e^{-i\kappa n}\psi_m\psi^*_{m-n}S^0_{nm}[|\alpha_q|^2e^{iqn}+|\beta_q|^2 - \alpha_a\beta^*_q e^{iqm}-\alpha^*_q\beta_q e^{iq(n-m)}], \tag{43}$$

$$\langle\Psi(\kappa)|\hat{H}^{\text{ex-ph}}|\Psi(\kappa)\rangle = -gN^{-1}\sum_{nmq} e^{-i\kappa n}\psi_m\psi^*_{m-n}S^0_{nm} \times[e^{iq(n-m)}(\alpha^*_a+\alpha_{-q}e^{-iqn})-(\beta^*_q+\beta_{-q})] - \frac{\phi}{2}\sum_{nm} e^{-i\kappa n}\psi_m(\psi^*_{m-n-1}S^{-1}_{nm}W^{-1}_{nm} + \psi^*_{m-n+1}S^{+1}_{nm}W^{+1}_{nm}), \tag{44}$$

where S^l_{nm} is the Debye-Waller factor, which has the usual physical meaning of quantifying overlaps between lattice wave functions,

$$S^l_{nm} = \exp\left\{N^{-1}\sum_q\left[|\alpha_q|^2(e^{iqn}-1)+|\beta_q|^2(e^{iql}-1) + \frac{1}{2}(e^{-iqn}+e^{-iql}-2)(\alpha_q\beta^*_q e^{iq(n+m)}+\alpha^*_q\beta_q e^{iq(n-m)})\right]\right\}. \tag{45}$$

The two auxiliary functions W^{-1}_{nm} and W^{+1}_{nm} are defined as

$$W^{+1}_{nm} = N^{-1}\sum_q(1-e^{iq})[e^{iq(n-m)}(\alpha^*_q+\alpha_q e^{-iqn}) - (\beta^*_q e^{-iq}+\beta_{-q})], \tag{46}$$

$$W^{-1}_{nm} = N^{-1}\sum_q(e^{-iq}-1)[e^{iq(n-m)}(\alpha^*_q+\alpha_q e^{-iqn}) - (\beta^*_q e^{iq}+\beta_{-q})]. \tag{47}$$

The Debye-Waller factor S^l_{nm} has a more complex form here than in more familiar cases owing to the distinct spatial relationships embodied in the two classes of phonon amplitudes,

$$S^{n_2-m_2}_{(n_1-m_1)(m_2-m_1)} \equiv \langle\Lambda^q_{n_1,n_2}|\Lambda^q_{m_1,m_2}\rangle, \tag{48}$$

where

$$|\Lambda^q_{m_1,m_2}\rangle = \exp\left\{-N^{-1/2}\sum_q[(\alpha_q e^{-iqm_1}-\beta_q e^{-iqm_2})b^+_q-\text{H.c.}]\right\} \times|0\rangle_{\text{ph}}. \tag{49}$$

We define the expectation value of the Hamiltonian in the GL Ansatz state as $E^{\kappa}=H^{\kappa}/M^{\kappa}$ where

$$H^{\kappa} = \langle\Psi(\kappa)|\hat{H}^{\text{ex}}+\hat{H}^{\text{ph}}+\hat{H}^{\text{ex-ph}}|\Psi(\kappa)\rangle. \tag{50}$$

The variational procedure minimizes the expectation values of the Hamiltonian in the GL Ansatz. Upon the conclusion of the optimization procedure, the variational parameters are determined, and exciton-phonon correlations in the optimal state are evaluated.

To obtain exact numerical solutions to a set of self-consistency equations born out of the variational principle, we adopt the relaxation iteration technique, an efficient method for identifying energy minima of a complex variational system.[33,34] The principal difficulties with this approach lie in the stability of the iteration and the quality of the convergence. Though a proper solution obtained by this or any other variational method must be stable relative to small changes in the variational parameters and that the search for such solutions relies upon this stability property, it is possible for errors in a fraction of the total solution to spread and destabilize the iteration or otherwise limit the quality of the convergence. Thus, while in principle the same family of solutions should result for randomly chosen initial data, in practice the best convergence results when the search is initialized with input that is already close to the solution being sought. For our problem, the mathematical dilemma of finding educated initial guesses for the nonlinear iterative scheme can be avoided for the most part due to the uniqueness of the physical solution and the availability of exact

TABLE I. Comparison of the ground-state energies in the absence of off-diagonal exciton-phonon coupling. Listed are results from three methods (the GL Ansatz, the Toyozawa Ansatz, and HA-DCPA) for two-parameter sets, $(J,g)=(1,1)$ $[(\gamma,\lambda)=(\frac{1}{2},\frac{1}{2})]$ and $(J,g)=(1,\sqrt{2})$ $[(\gamma,\lambda)=(\frac{1}{2},1)]$. Results from DMFT (Ref. 11), DMRG (Ref. 7), and Refs. 36 and 38 are also listed as a comparison.

Methods	$J=1$ $g=1$	$J=1$ $g=\sqrt{2}$
GL	−2.46931	−2.99802
Toyozawa	−2.46870	−2.99172
HA-DCPA	−2.46506	−2.98602
DMFT (Ref. 11)	−2.40	−2.89
DMRG (Ref. 7)	−2.46968	−2.99883
References 36 and 38	−2.46968472393287071561 (Ref. 38)	−2.998828186867 (Ref. 36)

solutions in certain limits of physical parameters. To achieve efficient and stable iterations toward the variational ground state, one may take advantage of the continuity of the ground state with respect to small changes in system parameters over much of the phase diagram and may initialize the iteration using a reliable ground state already determined at some nearby point in parameter space. Starting from those limits where exact solutions can be obtained analytically and executing a sequence of variations along well-chosen paths through the parameter space using solutions from one step to initialize the next, the whole parameter space can be explored.

IV. RESULTS AND DISCUSSIONS

In this section results from the HA-DCPA method and the GL Ansatz will be compared to arrive at a comprehensive understanding on the ground-state properties of generalized Holstein polaron at zero temperature. First, the energy spectra of the Holstein polaron are calculated for various strengths of off-diagonal exciton-phonon coupling. Based on the features from energy spectra, two- or three-dimensional phase diagrams spanned by electronic tunneling, diagonal coupling, and off-diagonal coupling are plotted, revealing the self-trapping transition. The pros and cons for the two methods are discussed in addition to making comparisons with the Toyozawa Ansatz.

Although the self-trapping transition is expected to be smooth on formal grounds,[35] it is commonplace for approximate treatments such as the GL and Toyozawa Ansätze to encounter discontinuities where polaron structure changes in too fast a fashion to be represented accurately within the scope of a specific computational method. The GL Ansatz, however, is expected to give a much smaller self-trapping region relative to the Toyozawa Ansatz in the three-dimensional parameter space spanned by (g,ϕ,J). Despite that the discontinuities near the self-trapping transition are primarily an artifact caused by the insufficient sophistication of the variational trial states, they do point to a real rapid change in the physical properties of the Holstein polaron with control parameters such as the exciton-phonon coupling strength and the exciton transfer integral.

Before we proceed to study the off-diagonal exciton-phonon coupling, the HA-DCPA method is first applied to diagonal-coupling-only cases. As mentioned earlier, the ground-state properties for the one-dimensional Holstein model have been extensively studied and several results for the ground-state energy are available for comparison.[8,36,37] Deserving mention is the variational approach in Ref. 36 which allows its variational space to be systematically expanded to achieve high accuracy on an infinite lattice. Furthermore, as known from our previous work, the GL Ansatz together with DMRG and the variational approach in Refs. 36 and 38 are arguably the most accurate ways to give the upper bound of the true ground-state energy. For comparison with the GL Ansatz and DMRG, we use HA-DCPA to calculate the ground-state energy for several typical cases, and results are listed in Table I. The two sets of control parameters represent two cases of intermediate coupling ($J=1$, $g=1$ and $J=1$, $g=\sqrt{2}$). Results from DMFT,[11] DMRG,[7] and Refs. 36 and 38 are listed in the table as a reference.

From Table I, the HA-DCPA energies are slightly higher than those of the GL Ansatz, the Toyozawa Ansatz, and the DMRG method; on the other hand, the results from the HA-DCPA method are lower in energy than that of DMFT. In the absence of off-diagonal coupling ϕ, the HA-DCPA method and the single-site DCPA method are supposed to yield the same coherent potential;[18] therefore the HA-DCPA result in Table I should coincide with Sumi's.[19] The DMFT method and the HA-DCPA method have many overlaps when applied to the Holstein model. The DMFT method is a powerful many-body technique to study electron-electron and electron-phonon interactions. In Ref. 11, DMFT was first applied to study the problem of a single electron coupled to Einstein phonons and discuss the structure of the small polaron consequently formed. It is suggested that the DMFT approach can provide an interpolation between known weak-coupling and strong-coupling results.[39] In the limit of a single electron or exciton interacting with a bath of phonons or disorder scatters, DMFT is reduced to the single-site DCPA method originally devised for inelastic-scattering processes in disordered systems. Furthermore, as demonstrated in Ref. 40, DCPA is equivalent to DMFT for strongly correlated electronic systems in a path-functional representation. Usually, a set of self-consistency equations in the DMFT and DCPA formulations are built from the assumption that the self-energy is independent of momentum. Since the self-energy functions for the single-particle excitations are independent of momentum in infinite dimensions,[41] these two

approximations (DMFT and DCPA) become exact in the infinite dimensions for translational invariant systems.

A. HA-DCPA method

Using the HA-DCPA approach, we can not only evaluate the ground-state properties but also extract information of the higher-energy excited state by solving the one-exciton Green's function. The introduction of the off-diagonal coherent potential in the HA-DCPA method makes it feasible to study in the presence of off-diagonal exciton-phonon coupling the self-trapping transition, in which dramatic changes in polaron properties are expected to happen with small changes in exciton-phonon coupling.[42] Landau[43] was the first to point out the rapid transition between the nearly free exciton in the weak-coupling regime and the self-trapped exciton in a strong-coupling regime. Furthermore, DCPA studies also revealed that these two polaron states may coexist in the crossover region identified with the self-trapping transition.[19]

Now let us see the effect of varying the off-diagonal coupling ϕ on the energy spectrum with the values of g and J fixed ($J=2$ and $g=1.0$ as an example). The value of ϕ goes from 0.0 to 2.5, and calculated polaron energy bands are displayed in Fig. 1. In the limiting case of $\phi=0.0$, shown in Fig. 1(a), the lowest-energy band shows a crossover from a nearly free exciton band to the one-phonon continuum at a critical value of the crystal momentum k_c, a typical feature in the weak diagonal-coupling regime.[44] In the limit of $g \to 0^+$ ($\phi=0.0$), k_c is given by $2J[1-\cos(k_c)]=\hbar\omega$.

As shown in Fig. 1(b), the case of $\phi=1.5$ reveals a visible energy gap between the top of the nearly free exciton band and the bottom of the one-phonon continuum. The lowest-energy band has a reduced width (compared to $\phi=0$), and above the one-phonon continuum, there appears the next lowest-energy band with a more reduced width. In the weak coupling and adiabatic limit and in the absence of ϕ, the gap size can be scaled in terms of g/J for one- or two-dimensional case.[45] The appearance of the second lowest-energy band implies a kind of exciton-phonon bound states.[46]

With off-diagonal coupling strength ϕ increased to 2.0, the width of the lowest-energy band is further reduced, and the nearly free polaron state in Fig. 1(b) is turned into a self-trapped state with a diminished band width; simultaneously, there appears a nearly free exciton band beneath the one-phonon continuum, as shown in Fig. 1(c). That is, the self-trapped exciton is found to coexist with the nearly free exciton. Such a phenomenon has been demonstrated in one dimension by a self-trapping mechanism with two quasidegenerate exciton levels, where the off-diagonal exciton-phonon coupling is regarded to play a key role for understanding the optical spectra of quasi-one-dimensional anthracene pyromellitic acid dianhydride.[47]

If ϕ is increased to 2.5 and 3.0, as plotted in Figs. 1(d) and 1(e), respectively, the self-trapped exciton with the lowest energy is left with very little dispersion. As a result, the width of the one-phonon continuum also vanishes. Below the one-phonon continuum in Fig. 1(d), there are altogether three bands, the lowest two with a bimodal structure, in agreement with results of the GL Ansatz to be presented later.

Based on the above analysis, the polarons can be roughly classified into three types according to the features of energy spectra below one-phonon continuum as follows: (I) a partial or full band for the nearly free exciton; (II) a full band for the lowest-energy state plus a partial band for the next lowest-energy state; (III) several full bands for self-trapped polaron states. A g-ϕ phase diagram with $J=2.0$ is plotted in Fig. 2. Horizontal and vertical coordinates represent diagonal and off-diagonal coupling strengths, respectively. Three regions labeled by I, II, and III correspond to the three classifications given above. The phase diagram in Fig. 2 shows a crossover region where the free exciton and the self-trapped exciton coexist.

In Fig. 3 we display the spectral density function at zero crystal momentum $A(k=0,E)$ for the same set of control parameters as in Figs. 1(a)–1(e), i.e., $J=2.0$, $g=1.0$, and $\phi=0.0$, 1.5, 2.0, 2.5, and 3.0, respectively. The spectral density functions displayed are normalized to unity with delta function broadened by an imaginary part of 0.01. The spectral functions for $\phi=0.0$ and 1.5, shown in Figs. 3(a) and 3(b), respectively, include a strong exciton peak and a weak broad phonon sideband one phonon energy higher. For $\phi=1.5$, there are three main peaks with an energy separation of one as shown in Fig. 3(b). This may be regarded as higher-energy vibronic states associated with a nearly free exciton.[19] For the intermediate cases shown in Fig. 3(c) ($\phi=2.0$) and Fig. 3(d) ($\phi=2.5$), the spacing between the lowest peak and the next lowest is smaller than one due to one partial band ($\phi=2.0$) or a set of full and partial bands ($\phi=2.5$) that emerge below the one-phonon continuum as ϕ is increased. Except for the lowest-energy peak at 7.88, which corresponds to a self-trapped state, the spectrum of $\phi=3.0$ is analogous to that of $\phi=2.5$ in overall spectral shape with the entire spectrum minus the tiny peak at 7.88 redshifted by 0.58 from the full $\phi=2.5$ spectrum.

The addition of off-diagonal coupling to the traditional molecular crystal model adds rich structures to the spectral functions, and as a consequence, it is not surprising that off-diagonal coupling plays a crucial role in the optical properties of organic molecular crystals. In his early work Sumi[6] emphasized the importance of off-diagonal interactions between the electronic excitation of each molecular and the phonons representing the mutual slide and approach of the next-nearest pair of molecules. Furthermore, he used a comprehensive exciton-phonon coupling model inclusive of off-diagonal coupling to explain with great success the origins of yellow emission from α perylene as well as violet emission from supercooled pyrene.

B. GL Ansatz

To understand the self-trapping phase diagram in the simultaneous presence of diagonal and off-diagonal couplings, we take three cross sections of a three-dimensional crossover region of the phase diagram, namely, three planes determined by $J=2.0$, $J=3.0$, and $J=4.0$ in the parameter space spanned by J, g, and ϕ. The result we obtain is three spear-shaped regions in the three panels of Fig. 4.

Inside (outside) the spear-shaped regions in Fig. 4, two (one) convergent solutions are found for the set of self-

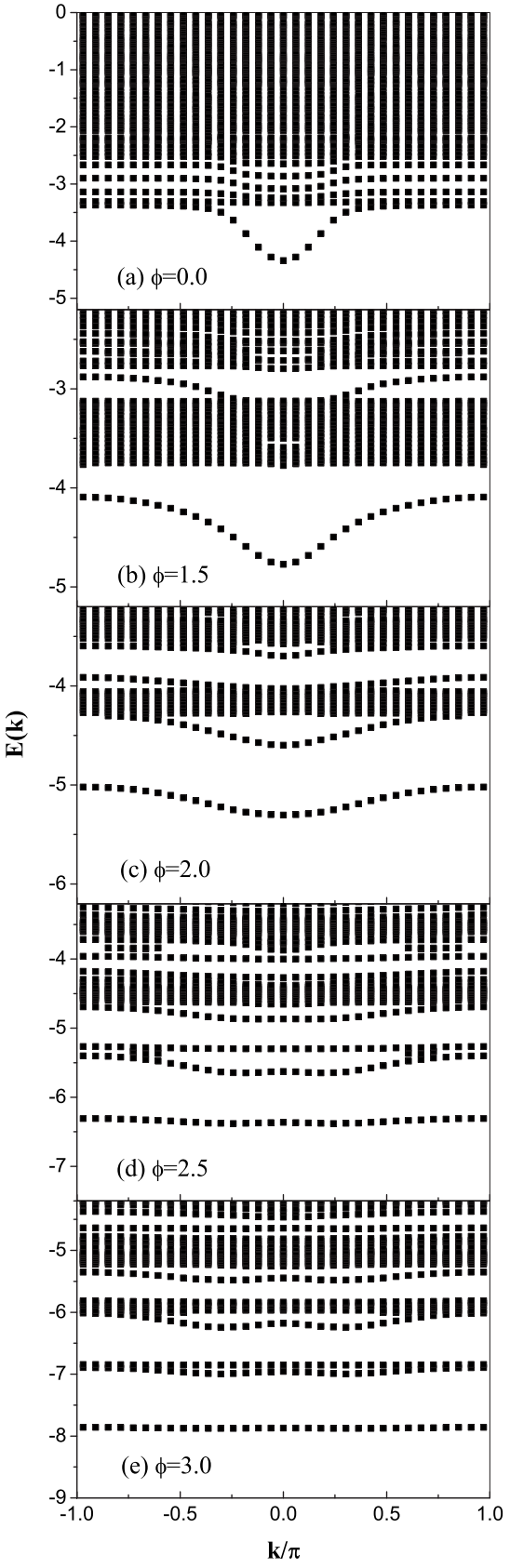

FIG. 1. Polaron dispersion curves calculated by the HA-DCPA method are plotted for $(J,g)=(2.0,1.0)$ $[(\gamma,\lambda)=(\frac{1}{4},\frac{1}{4})]$ and five values of ϕ: (a) $\phi=0.0$, (b) $\phi=1.5$, (c) $\phi=2.0$, (d) $\phi=2.5$, and (e) $\phi=3.0$.

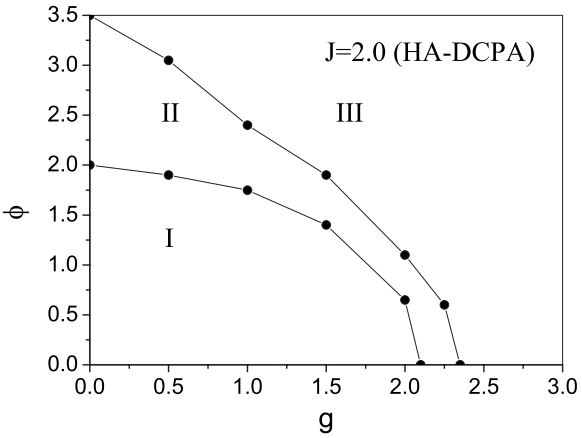

FIG. 2. Phase diagram in the two-dimensional space spanned by g and ϕ is generated from the energy spectra calculated by the HA-DCPA method for the case of $J=2.0$.

consistency equations in the iterative variational procedure depending whether the equations are solved using a small-polaron-type initialization or a large-polaron-type one. This spear-shaped area is defined as the self-trapping region since exciton-phonon correlations undergo drastic changes as this area is traversed in the parameter space. We find that the self-trapping regions associated with the GL Ansatz (solid line) fall within those associated with the Toyozawa Ansatz (dashed line) for all three values of exciton transfer integral J displayed in Fig. 4, and the reduction in the size of the self-trapping regions achieved by the GL Ansatz increases with increasing J. With increasing transfer integral J, the self-trapping region expands toward the large g area.

The variational energies in the simultaneous presence of diagonal and off-diagonal couplings based on the GL Ansatz have been significantly lowered as compared with the Toyozawa Ansatz owing to the introduction of the second set of phonon displacement parameter β_q^κ. Below we will discuss variational energy bands and analyze detailed phonon displacements and exciton magnitudes for a few specific points marked by stars in Fig. 4.

Polaron energy bands for four phase-space points marked as stars in Fig. 4(b) are shown in Fig. 5. The point $(J,g,\phi)=(3.0,2.0,2.0)$ sits in the upper portion of the g-ϕ plane with $J=3.0$. A combination of large diagonal and off-diagonal couplings narrows the polaron energy band substantially compared with the bare exciton band and the corresponding effective mass of polaron much heavier than that of the bare exciton, resulting in a small polaron. The minimum-energy points are found at $\kappa=\pm 0.4375\pi$ thanks to the presence of off-diagonal coupling. With the off-diagonal coupling strength reduced to $\phi=0.5$, the point $(J,g,\phi)=(3.0,2.0,0.5)$ now is located below the spear-shaped self-trapping region in Fig. 4(b). This is a case of large polaron with a much-increased polaron bandwidth and a substantially lighter polaron mass. The energy bands calculated by the GL and Toyozawa Ansätze are shown in Fig. 5(b). The improvements made by the GL Ansatz over the Toyozawa Ansatz increase as one goes from the zone center to the zone boundary. With the diagonal coupling strength reduced to $g=1$ from the initial starting position of $(J,g,\phi)=(3.0,2.0,2.0)$,

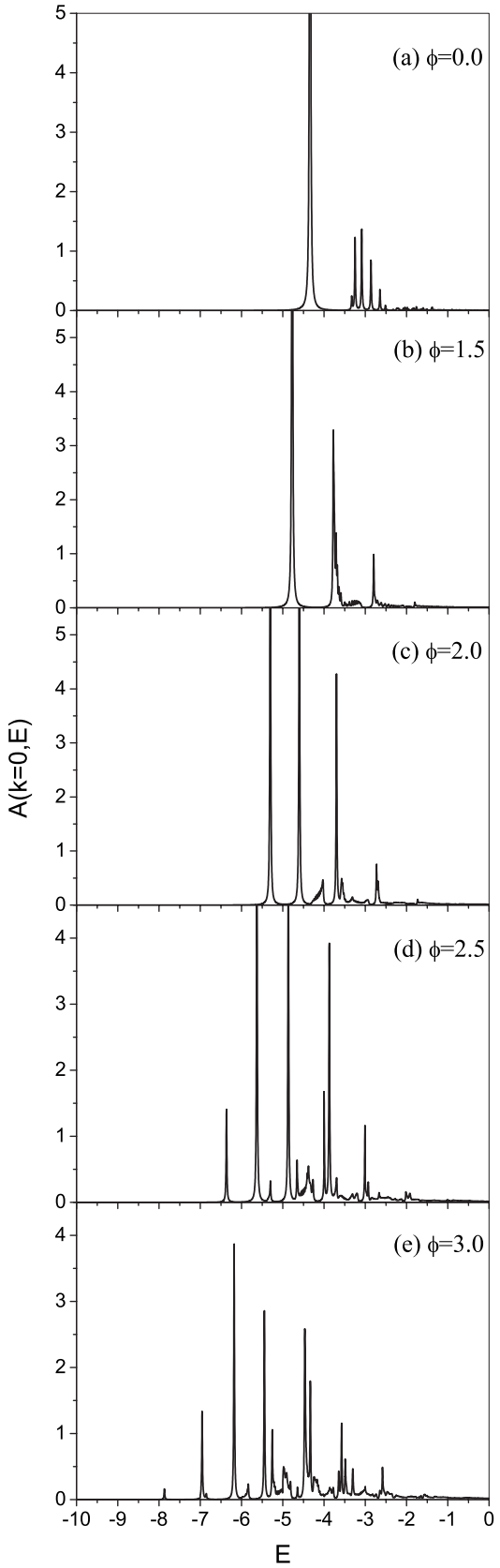

FIG. 3. The spectral density function $A(k=0,E)$ calculated with the HA-DCPA method for $(J,g)=(2.0,1.0)$ $[(\gamma,\lambda)=(\frac{1}{4},\frac{1}{4})]$ and five values of ϕ: (a) $\phi=0.0$, (b) $\phi=1.5$, (c) $\phi=2.0$, (d) $\phi=2.5$, and (e) $\phi=3.0$.

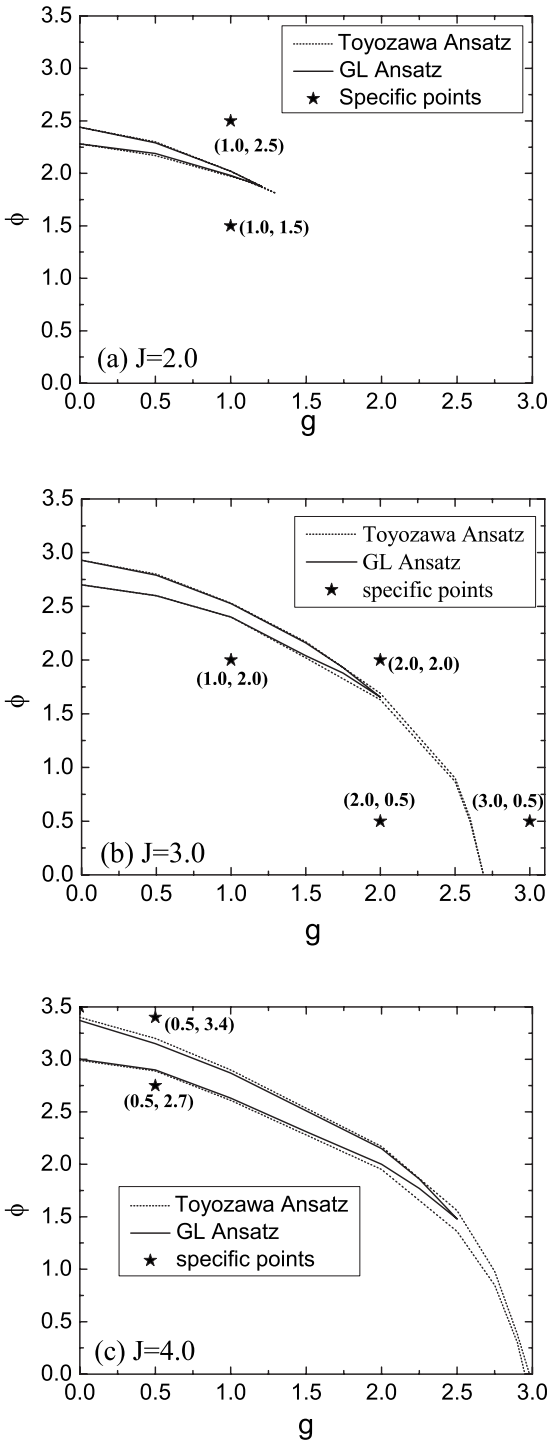

FIG. 4. Two-dimensional g-ϕ phase diagrams of the zone-center self-trapping transition for (a) $J=2.0$, (b) $J=3.0$, and (c) $J=4.0$. Two methods are compared: the GL Ansatz (solid line) and the Toyozawa Ansatz (dotted line).

the point $(J,g,\phi)=(3.0,1.0,2.0)$, slightly below the spear-shaped self-trapping boundary, is a case of weak diagonal coupling and moderate off-diagonal coupling. Surprisingly, the energy minimum is at the zone center $\kappa=0$ as shown in Fig. 5(c), unlike in Fig. 5(a) (the case of a stronger g). The advantage of the GL Ansatz over the Toyozawa Ansatz measured by the reduction in energy seems at a minimum for this

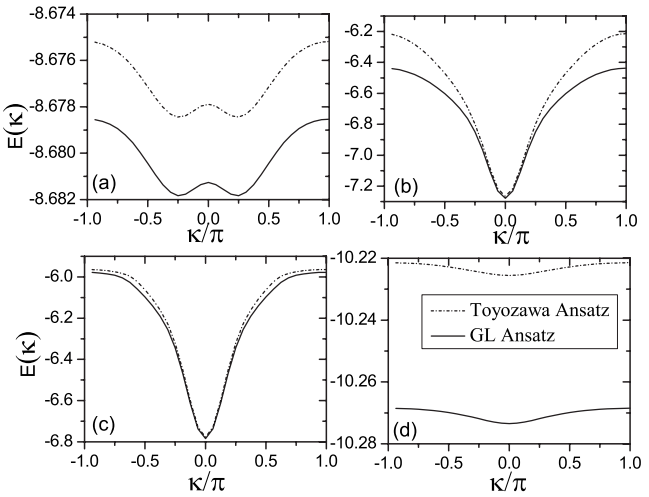

FIG. 5. Polaron energy bands calculated with the GL Ansatz (solid line) and the Toyozawa Ansatz (dashed-dotted line) for the four points in Fig. 4(b) labeled by stars: (a) $J=3.0$, $g=2.0$, $\phi=2.0$; (b) $J=3.0$, $g=2.0$, $\phi=0.5$; (c) $J=3.0$, $g=1.0$, $\phi=2.0$; (d) $J=3.0$, $g=3.0$, $\phi=0.5$.

set of control parameters. The point $(J,g,\phi)=(3.0,3.0,0.5)$ is a case of an obvious small-polaron character, and since the exciton phonon is primarily diagonal with $g=3.0$, the polaron band has a minimum at the zone center $\kappa=0$ as shown in Fig. 5(d).

In Table II, we compare the lowest energies of the polaron band $E(\kappa)$ calculated by the GL and Toyozawa Ansätze and by the HA-DCPA method for all eight points in Fig. 4 marked as stars. Four out of the eight are from Fig. 4(b), and their polaron energy bands have been displayed in Fig. 5. Overall, the ground-state energy $E(\kappa)$ from the GL Ansatz is superior to that from the Toyozawa Ansatz as expected. In addition, the HA-DCPA method gives a lower ground-state energy than those obtained variationally in the portion of the parameter space characterized by the large polaron; while in the region characterized by the small polaron, the GL and Toyozawa Ansatz have lower, and therefore, more accurate ground-state energies due to the fact that the true ground energy always lies below its variational upper bounds.

The lowest polaron energy bands calculated by the GL Ansatz, the Toyozawa Ansatz, and the HA-DCPA method are displayed in Fig. 6 for five points in the parameter space labeled by the stars in Fig. 4, namely, $(J,g,\phi)=(2.0,1.0,1.5)$, $(3.0,1.0,2.0)$, $(4.0,0.5,2.7)$, $(3.0,2.0,2.0)$, and $(2.0,1.0,2.5)$. First, comparisons of lowest polaron energies are made among the three approaches in the weak-coupling regime for all crystal momenta. It is found that the HA-DCPA method generates polaron bands that are lower in energy and smaller in bandwidth for the three weak-coupling points $(J,g,\phi)=(2.0,1.0,1.5)$, $(3.0,1.0,2.0)$, and $(4.0,0.5,2.7)$. Since the HA-DCPA bands can fall below the true ground-state energy bands, no definitive conclusion can be drawn here on whether the HA-DCPA results are indeed superior. By increasing the diagonal or off-diagonal coupling strength, however, the GL and Toyozawa Ansätze can yield much lower polaron energy bands than the HA-DCPA method, as clearly demonstrated by Figs. 6(d) and 6(e) for the two points $(J,g,\phi)=(3.0,2.0,2.0)$ and $(2.0,1.0,2.5)$, respectively. Furthermore, near the self-trapped transition, the HA-DCPA energy bands are smooth as shown in Fig. 6(c), while those from the variational approaches display a discontinuity which corresponds to the crossover between the large and small polarons. Despite that the GL variational method gives a relatively precise identification for the self-trapping transition, awkward discontinuities in energy bands still exist near the critical crystal momenta that separate a nearly free exciton near the zone center from a polaron state near the zone boundary that contains mostly one-phonon plane waves. More sophisticated trial states, such as the one constructed from Davydov's D1 Ansatz, are now being developed for both diagonal and off-diagonal exciton-phonon couplings and may help resolve those difficult issues with more certainty.

Variational methods, such as the GL and Toyozawa Ansätze being employed here, provide a large amount of structural information on exciton-phonon correlations after the complete set of optimized variational parameters is obtained at the end of the iterative procedure. For the GL Ansatz, these parameters are the two components of the phonon displacements, α_q^κ and β_q^κ, plus the real and imaginary parts of the exciton amplitudes, Re ψ_n^κ and Im ψ_n^κ. These variational parameter matrices are shown in Figs. 7–10 for four sets of control parameters, $(J,g,\phi)=(3.0,2.0,2.0)$, $(3.0,1.0,2.0)$, $(4.0,0.5,2.7)$, and $(4.0,0.5,3.4)$, respectively.

We discuss first a case of strong exciton-phonon coupling with $J=3.0$, $g=2.0$, and $\phi=2.0$. Exciton-phonon correlations

TABLE II. Comparison of the lowest energies in the polaron energy bands calculated with the GL Ansatz, the Toyozawa Ansatz, and the HA-DCPA method for the eight points marked by stars in Fig. 4.

J	g	ϕ	GL	Toyozawa	HA-DCPA	κ
2.0	1.0	1.5	−4.7266	−4.7224	−4.7724	0
2.0	1.0	2.5	−6.8552	−6.8506	−6.3628	$\pm 0.4375\pi$
3.0	1.0	2.0	−6.7837	−6.7766	−6.8443	0
3.0	2.0	0.5	−7.2795	−7.2658	−7.2195	0
3.0	2.0	2.0	−8.6818	−8.6784	−8.6684	$\pm 0.25\pi$
3.0	3.0	0.5	−10.2735	−10.2256	−10.2554	0
4.0	0.5	2.7	−8.7535	−8.7397	−8.8163	0
4.0	0.5	3.4	−10.7796	−10.7711	−9.4406	$\pm 0.5\pi$

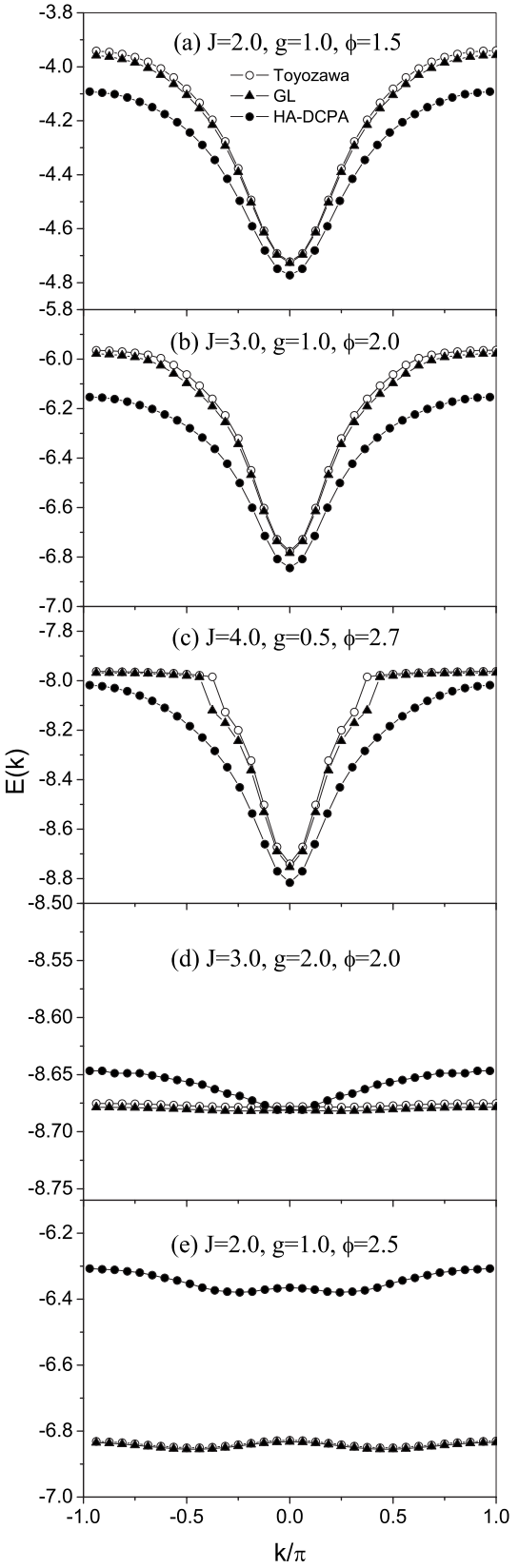

FIG. 6. Lowest polaron energy bands calculated with the Toyozawa Ansatz (hollow circles), the GL Ansatz (solid triangles), and the HA-DCPA method (solid circles) for (a) $J=2.0$, $g=1.0$, $\phi=1.5$; (b) $J=3.0$, $g=1.0$, $\phi=2.0$; (c) $J=4.0$, $g=0.5$, $\phi=2.7$; (d) $J=3.0$, $g=2.0$, $\phi=2.0$; (e) $J=2.0$, $g=1.0$, $\phi=2.5$.

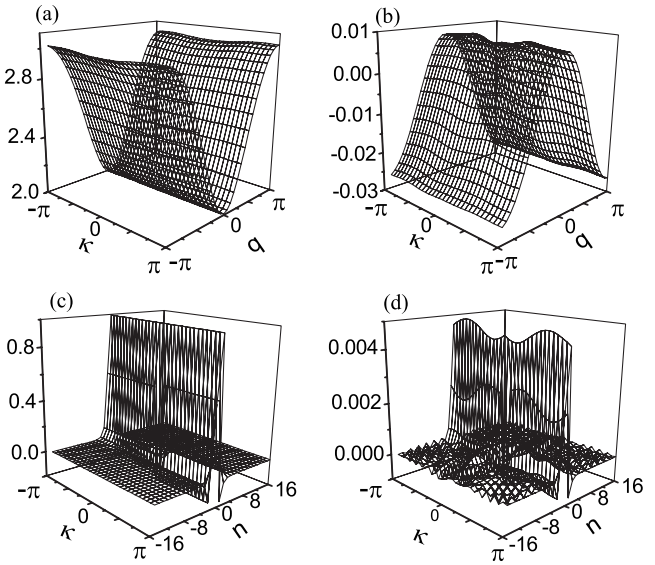

FIG. 7. Optimized variational parameters of the GL Ansatz for the case $J=3.0$, $g=2.0$, $\phi=2.0$; (a) α_q^κ, (b) β_q^κ, (c) Re ψ_n^κ, (d) Im ψ_n^κ.

are determined by the phonon displacements and the exciton amplitudes. As shown in Fig. 7, phonon displacements α_q^κ and β_q^κ are essentially independent of the joint crystal momentum κ, a signature of small polaron, and both have a sinusoidal modulation with respect to the phonon momentum, reflecting a slight spreading of the lattice distortion to nearest neighbors but very little beyond. Most of the phonon displacements are carried by the α_q^κ component, with only a small portion being allocated to the β_q^κ component. The real part of the exciton amplitude is essentially independent of κ with most of the amplitude localized on a single site $n=0$, and the imaginary part Im ψ_n^κ in this case is very small except for $n=0$.

A case of the weak diagonal coupling and moderate off-diagonal coupling with $J=3.0$, $g=1.0$, and $\phi=2.0$ is consid-

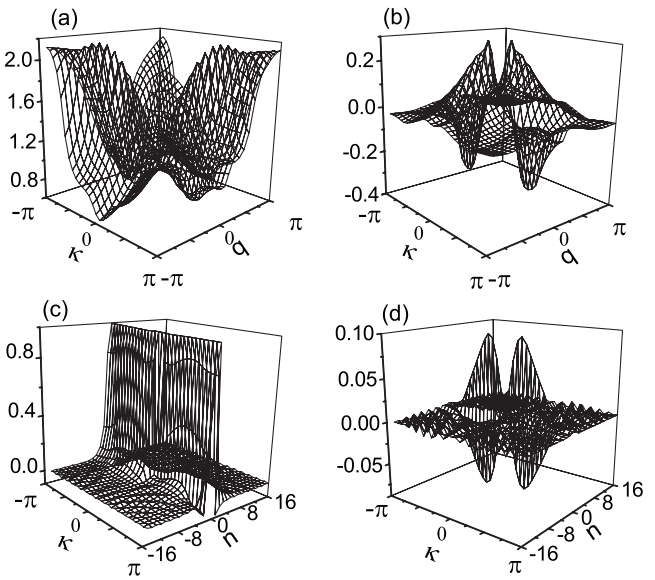

FIG. 8. Optimized variational parameters of the GL Ansatz for the case $J=3.0$, $g=1.0$, $\phi=2.0$; (a) α_q^κ, (b) β_q^κ, (c) Re ψ_n^κ, (d) Im ψ_n^κ.

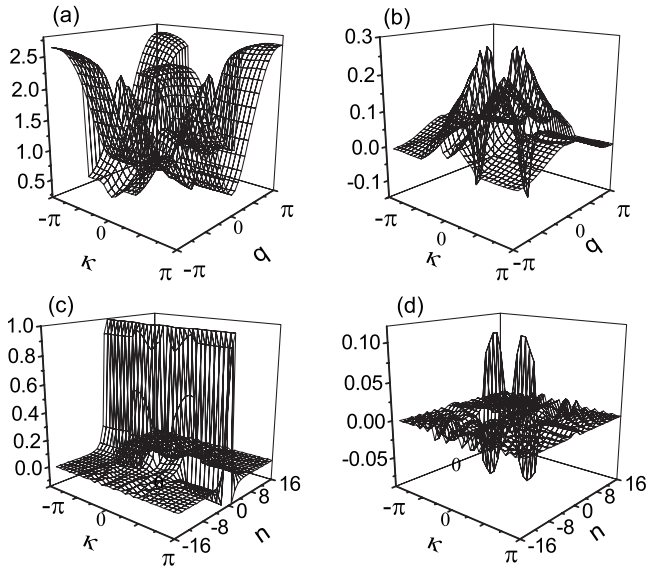

FIG. 9. Optimized variational parameters of the GL Ansatz for the case $J=4.0$, $g=0.5$, $\phi=2.7$; (a) α_q^κ, (b) β_q^κ, (c) Re ψ_n^κ, (d) Im ψ_n^κ.

ered in Fig. 8. The secondary phonon displacement β_q^κ has grown in both absolute and relative strengths and has acquired a distinctive shape. The primary phonon displacement α_q^κ has a small pulse-shaped component appearing along the

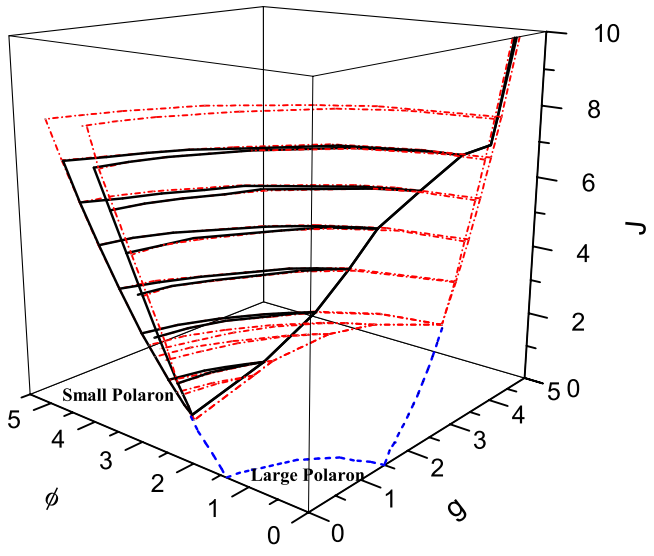

FIG. 10. (Color online) Phase diagram for the zone-center self-trapping transition in the three-dimensional g-ϕ-J space for the GL Ansatz (solid line) and the Toyozawa Ansatz (dashed-dotted line). Supplementary boundaries from quantum-information considerations (Ref. 48) are shown in the low-J region as well as on the g-ϕ plane (dashed line). Combined, the three-dimensional self-trapping boundaries approximately divide the g-ϕ-J space into two portions, namely, the large-polaron part in the front with weak (diagonal or off-diagonal) coupling and the small-polaron part in the back with strong (diagonal or off-diagonal) coupling. In the $g=0$ plane, we have $J_c=1.2$ and $\phi_c=1.97$ for the Toyozawa Ansatz and $J_c=1.3$ and $\phi_c=2.01$ for the GL Ansatz; in the $\phi=0$ plane, we have $J_c'=3.0$ and $g_c'=2.69$ for the Toyozawa Ansatz and $J_c'=7.34$ and $g_c'=3.69$ for the GL Ansatz.

diagonal line $q=\kappa$ (the sharp "dinosaur back" on the ridges), signaling a one-phonon plane wave and therefore a large-polaron characteristic. Moreover, α_q^κ and β_q^κ amplitudes vary considerably with the crystal momentum κ, reflecting a strong momentum sensitivity, with their characteristic magnitudes subject to the sum rule $\alpha_{q=0}+\beta_{q=0}=g$. The real part profile of exciton magnitude is also pulse shaped and nearly independent of κ, and its amplitude displays the appropriate symmetric property, e.g., Re ψ_n^κ=Re ψ_{-n}^κ while the very small imaginary part is antisymmetric, e.g., Im ψ_n^κ=−Im ψ_{-n}^κ.

At a larger value of the exciton transfer integral, $J=4.0$, and a combination of weak diagonal coupling and stronger off-diagonal coupling $(g=0.5, \phi=2)$, the complete solution set is presented in Fig. 9. The corresponding GL polaron energy band has been shown in Fig. 6(c). This exciton-phonon system in this case has a large-polaron character for many values of κ near the zone center. Due to the fact that this set of control parameters lies very close to the self-trapping region in the three-dimensional parameter space, there exist discontinuities in the optimized variational parameters as one goes from the zone center to the zone boundary. This is most obvious in the primary phonon displacement α_q^κ; at small $|\kappa|$, it behaves as a large polaron, while at large $|\kappa|$ adopts the characteristic of a small polaron.

A three-dimensional phase diagram is generated by the variational methods to facilitate understanding of the polaron self-trapping transition in the simultaneous presence of diagonal and off-diagonal exciton-phonon couplings. Such a phase diagram showing polaron self-trapping near the zone center in the three-dimensional parameter space spanned by (g, ϕ, J) is displayed in Fig. 10. The curved boundary surfaces shown by solid lines and dashed-dotted lines correspond to the self-trapping regions associated with the GL Ansatz and Toyozawa Ansatz, respectively. Within the curved boundary surfaces, two sets of solutions coexist near the zone center for the self-consistency equations that govern the variational parameters of the GL and Toyozawa Ansätze. Outside the self-trapping regions, only one unique set of solutions can be obtained for the self-consistency equations near zone center, but boundaries can still be drawn by calculating the quantum entanglement between the exciton and the phonons.[48] Supplementary boundaries from these quantum-information considerations are shown in the low-J region as well as on the g-ϕ plane by the dashed lines. Combined, the three-dimensional self-trapping boundaries approximately divide the g-ϕ-J space into two portions, namely, the large-polaron part in the front with weak exciton-phonon coupling and the small-polaron part in the back with strong exciton-phonon coupling.

From the phase diagram of Fig. 10, we find that the onset of the aforementioned polaronic self-trapping bistability occurs at critical values of exciton hopping integral, diagonal, and off-diagonal couplings. For examples, in the $g=0$ plane, we have $J_c=1.2$ and $\phi_c=1.97$ for the Toyozawa Ansatz and $J_c=1.3$ and $\phi_c=2.01$ for the GL Ansatz; in the $\phi=0$ plane, we have $J_c'=3.0$ and $g_c'=2.69$ for the Toyozawa Ansatz and $J_c'=7.34$ and $g_c'=3.69$ for the GL Ansatz. For small values of J, the transition from small polaron to large polaron is smooth for both Ansätze.

For a given J value that is sufficiently large, we observe that in the g-ϕ plane the spear-shaped self-trapping region of

the GL Ansatz is much smaller than that of the Toyozawa Ansatz (cf. Fig. 4). One would expect the principal feature of such a two-dimensional phase diagram in the g-ϕ plane to be a boundary line separating a small-polaron region from a large-polaron region associated with the common notion of a self-trapping transition. In reality, we have encountered spear-shaped regions in the two-dimensional phase diagram here. It is not surprising for approximate treatments such as ours to encounter discontinuities where polaron structure changes in too complex too rapid a fashion to be captured numerically in its entirety. From this viewpoint, the GL Ansatz is not an exception, but it has its merit to yield a much smaller self-trapping volume relative to the Toyozawa Ansatz in the three-dimensional parameter space spanned by (g,ϕ,J).

V. CONCLUSION

We have investigated the generalized Holstein model employing two different approaches, the GL Ansatz and the HA-DCPA method. The HA-DCPA method is realized by replacing exciton-phonon interactions using a nonlocal translationally invariant coherent potential, which is determined by assuming that the $\hat{T}$ matrix associated with the perturbation part in the original Hamiltonian vanishes under the thermal average of phonon scattering. Compared with other numerical methods, e.g., the slightly complicated diagrammatic QMC,[13] the HA-DCPA method is relatively easy to implement because the key coherent potential can be determined by a formal recursive relation regardless of the detailed forms of the exciton-phonon interactions. The HA-DCPA approach allows us to calculate ground-state properties as well as spectral density functions and energy spectra. Furthermore, it can be easily extended to finite temperatures. Information extracted on dynamic properties of the Holstein polaron by the HA-DCPA method is complementary to that on ground-state properties provided by the variational approaches such as the GL and Toyozawa Ansätze.

Compared with the Toyozawa Ansatz, the GL Ansatz gains noticeable improvement in the ground-state energy of the Holstein polaron with simultaneous diagonal and off-diagonal exciton-phonon couplings, and the introduction of the secondary phonon displacement β_q^κ allows a substantial reduction in the self-trapping region in the three-dimensional parameter space in which two sets of convergent solutions are found for the self-consistency equations. Using the GL method, we have presented a phase diagram in three dimensions spanned by electronic tunneling, diagonal coupling, and off-diagonal coupling for the self-trapping transition near the zone center. Detailed structures of exciton-phonon correlations have been illustrated for several sets of control parameters in the small-polaron, large-polaron, and crossover regimes by displaying optimized exciton amplitudes as well as primary and secondary phonon displacements.

The HA-DCPA method also helps reveal the evolution of energy spectra and spectral density functions with off-diagonal coupling interaction. In the weak off-diagonal coupling limit, the HA-DCPA method is reduced to the single-site DCPA. In the sizable area near the self-trapping line in the parameter space, self-trapped states and nearly free exciton-polaron states below the one-phonon continuum are found to coexist.

ACKNOWLEDGMENTS

Support from the Singapore Ministry of Education through the Academic Research Fund (Tier 2) under Project No. T207B1214 is gratefully acknowledged.

*yzhao@ntu.edu.sg

[1] Y. Zhao, D. W. Brown, and K. Lindenberg, J. Chem. Phys. **100**, 2335 (1994).
[2] Y. Zhao, D. W. Brown, and K. Lindenberg, J. Chem. Phys. **106**, 2728 (1997).
[3] Y. Zhao, Ph.D. thesis, University of California, San Diego, 1994.
[4] V. M. Stojanovic, P. A. Bobbert, and M. A. J. Michels, Phys. Rev. B **69**, 144302 (2004).
[5] L. A. Dissado and S. H. Walmsley, Chem. Phys. **86**, 375 (1984).
[6] H. Sumi, Chem. Phys. **130**, 433 (1989).
[7] E. Jeckelmann and S. R. White, Phys. Rev. B **57**, 6376 (1998).
[8] Y. Zhao, D. W. Brown, and K. Lindenberg, J. Chem. Phys. **107**, 3159 (1997); **107**, 3179 (1997); **106**, 5622 (1997); A. Romero, D. W. Brown, and K. Lindenberg, *ibid.* **109**, 6540 (1998).
[9] H. B. Shore and L. M. Sander, Phys. Rev. B **7**, 4537 (1973).
[10] A. S. Alexandrov, V. V. Kabanov, and D. K. Ray, Phys. Rev. B **49**, 9915 (1994).
[11] S. Ciuchi, F. de Pasquale, S. Fratini, and D. Feinberg, Phys. Rev. B **56**, 4494 (1997).
[12] H. De Raedt and A. Lagendijk, Phys. Rev. B **27**, 6097 (1983).
[13] N. V. Prokof'ev and B. V. Svistunov, Phys. Rev. Lett. **81**, 2514 (1998).
[14] G. L. Goodvin, M. Berciu, and G. A. Sawatzky, Phys. Rev. B **74**, 245104 (2006).
[15] A. S. Mishchenko, N. V. Prokof'ev, A. Sakamoto, and B. V. Svistunov, Phys. Rev. B **62**, 6317 (2000).
[16] M. Berciu and G. L. Goodvin, Phys. Rev. B **76**, 165109 (2007).
[17] Y. Toyozawa, Prog. Theor. Phys. **26**, 29 (1961).
[18] T. Kato, F. Sasaki, and S. Kobayashi, Chem. Phys. Lett. **303**, 649 (1999).
[19] H. Sumi, J. Phys. Soc. Jpn. **36**, 770 (1974); **38**, 825 (1975).
[20] T. Kato and S. Kobayashi, J. Lumin. **87-89**, 281 (2000).
[21] T. Holstein, Ann. Phys. (N.Y.) **8**, 325 (1959).
[22] T. Holstein, Ann. Phys. (N.Y.) **8**, 343 (1959).
[23] P. Soven, Phys. Rev. **156**, 809 (1967).
[24] D. W. Taylor, Phys. Rev. **156**, 1017 (1967).
[25] B. Velicky, S. Kirkpatrick, and H. Ehrenreich, Phys. Rev. **175**, 747 (1968).
[26] S. V. Izvekov, Phys. Solid State **39**, 1383 (1997).
[27] R. E. Lagos and R. A. Friesner, Phys. Rev. B **29**, 3045 (1984).
[28] S. Abe, J. Phys. Soc. Jpn. **57**, 4029 (1988).
[29] D. J. Evans and G. P. Morriss, *Statistical Mechanics of Nonequi-*

librium Liquids (Academic, London, 1990).
[30] M. Cini and D. Andrea, J. Phys. C **21**, 193 (1988).
[31] R. E. Merrifield, J. Chem. Phys. **40**, 445 (1964).
[32] Y. Zhao, G. Q. Li, J. Sun, and W. H. Wang, J. Chem. Phys. **129**, 124114 (2008).
[33] Y. Zhao and H. N. Bertram, J. Magn. Magn. Mater. **114**, 329 (1992).
[34] Y. Zhao and H. N. Bertram, J. Appl. Phys. **77**, 6411 (1995).
[35] H. Löwen, Phys. Rev. B **37**, 8661 (1988).
[36] J. Bonča, S. A. Trugman, and I. Batistić, Phys. Rev. B **60**, 1633 (1999).
[37] Y. Cheng and R. J. Silbey, J. Chem. Phys. **128**, 114713 (2008).
[38] L. C. Ku, S. A. Trugman, and J. Bonca, Phys. Rev. B **65**, 174306 (2002).
[39] A. Georges, G. Kotliar, W. Krauth, and M. J. Rozenberg, Rev. Mod. Phys. **68**, 13 (1996).
[40] Y. Kakehashi, Phys. Rev. B **66**, 104428 (2002).
[41] W. Metzner and D. Vollhardt, Phys. Rev. Lett. **62**, 324 (1989).
[42] A. S. Mishchenko and N. Nagaosa, J. Phys. Soc. Jpn. **75**, 011003 (2006).
[43] L. D. Landau, Phys. Z. Sowjetunion **3**, 664 (1933).
[44] G. Whitfield and R. Puff, Phys. Rev. **139**, A338 (1965).
[45] S. Engelsberg and J. R. Schrieffer, Phys. Rev. **131**, 993 (1963).
[46] Y. Toyozawa and J. Hermanson, Phys. Rev. Lett. **21**, 1637 (1968); J. C. Hermanson, Phys. Rev. B **2**, 5043 (1970).
[47] A. S. Mishchenko and N. Nagaosa, Phys. Rev. Lett. **86**, 4624 (2001).
[48] Y. Zhao, P. Zanardi, and G. Chen, Phys. Rev. B **70**, 195113 (2004).